Cobalt Sulfide Nanofilm-assembled Cube as an Efficient Catalyst for Activating Monopersulfate to degrade UV Filter, 4,4'-Dihydroxybenzophenone, in Water

Jhih-Yang Yin[a], *Wen Da Oh*[b], *Eilhann Kwon*[c], *Bui Xuan Thanh*[d], *Siming You*[e], *Haitao Wang*[f,*] *and Kun-Yi Andrew Lin*[a,*]

[a]Department of Environmental Engineering & Innovation and Development Center of Sustainable Agriculture, National Chung Hsing University, 250 Kuo-Kuang Road, Taichung, Taiwan

[b]School of Chemical Sciences, Universiti Sains Malaysia, 11800 Penang, Malaysia

[c]Department of Environment and Energy, Sejong University, 209 Neungdong-ro, Gunja-dong, Gwangjin-gu, Seoul, Republic of Korea

[d]Faculty of Environment and Natural Resources, Ho Chi Minh City University of Technology, VNU-HCM, 268 Ly Thuong Kiet, District 10, Ho Chi Minh City, 700000, Viet Nam

[e]James Watt School of Engineering, University of Glasgow, Glasgow G12 8QQ, UK

[f] Key Laboratory of Pollution Processes and Environmental Criteria, College of Environmental Science and Engineering, Nankai University, Tianjin 300071, P. R. China

*Corresponding Authors. E-mail addresses:linky@nchu.edu.tw (K. Lin); envwang@nankai.edu.cn (H. Wang)

Abstract

As hydroxylated benzophenones (HBPs) represent most typical UV filters and UV stabilizers, increasing release of HBPs into the aquatic environment has caused serious threats to the aquatic ecology. Among various HBPs, 4,4'-Dihydroxybenzophenone (4HBP) receives growing attentions as an emerging contaminant due to its potential toxicity of endocrine disrupting effect. For establishing useful techniques to remove 4HBP from water, this study, as the first study, aims to develop cobalt sulfide as a heterogeneous catalyst to activate monopersulfate (MPS) for generating sulfate radical ($SO_4^{\bullet-}$) to degrade 4HBP. Especially, a unique cubic assembly of cobalt sulfide nanofilms (CSNF) is developed through a simple sulfurization of Prussian Blue (PB) in the form of $Co_3[Co(CN)_6]_2$ to transform this PB to CSNF. Such a resulting CSNF exhibits much higher catalytic activities than the pristine PB, and the reference catalyst, Co_3O_4, for activating MPS to degrade 4HBP in terms of degradation extents and kinetics. With very low dosages of CSNF = 50 mg/L and MPS = 100 mg/L, 5 mg/L of 4HBP could be fully eliminated in 15 min, validating that CSNF is a promising catalyst for activating MPS to 4HBP. E_a of 4HBP degradation by CSNF-activated MPS is also determined as 68 kJ/mol. The activation mechanism and degradation pathway of 4HBP degradation by CSNF-activated MPS is investigated using electro paramagnetic resonance and mass spectrometer, respectively, to further to provide insights into degradation behaviors for developing optimal sulfate-radical-based advanced oxidation processes of 4HBP degradation.

Keywords: cobalt sulfide, monopersulfate, Dihydroxybenzophenone, UV filters, sulfate radical, emerging contaminant

1. Introduction

As chemical UV filters are intensively produced and consumed, increasing release of these chemical UV filters into the environment has caused serious concerns [1]. These chemical UV filters have been classified as emerging contaminants due to their potential toxicities and negative effects, including xenohormone which would disrupt reproductive activity [2-5].

Among various types of chemical UV filters, hydroxylated benzophenones (HBPs) represent the most common chemical UV filters [6]. Thus, HBPs have been continuously discharged into natural water bodies from aquatic activities [7], and thus easily detected in many water bodies [8, 9]. To avoid adverse impact and consequence of these HBPs in water, it is necessary to remove HBPs from polluted water bodies.

Although a few attempts have been made to control and eliminate HBPs, existing studies had been focused on 2,4'-Dihydroxybenzophenone (2HBP). However, an another important HBP, 4,4'-Dihydroxybenzophenone (4HBP), has also received enormous attentions due to its increasing and extensive consumption [10]. Nevertheless, no studies have been ever conducted to develop techniques for eliminating 4HBP from water and investigate degradation behaviors under various conditions as well as degradation pathway. Thus, the present study aims to be the first research for establishing useful processes to eliminate 4HBP from water.

As advanced oxidation processes (AOPs) have been validated as useful approaches to eliminate emerging contaminants [11], AOPs shall be also promising for degrading 4HBP. Especially, while hydroxyl radical ($^{\bullet}OH$)-based AOPs have been extensively employed for degrading emerging contaminants, recently sulfate radical ($SO_4^{\bullet-}$)-based AOPs receive growing attention for degrading emerging contaminants [12] because $SO_4^{\bullet-}$ could exhibit higher oxidation potentials than $^{\bullet}OH$ with longer half-life [13].

For obtaining $SO_4^{\bullet-}$, monopersulfate (MPS) appears as a popular source as MPS is industrially-available, inexpensive, and environmentally friendly [14]. However, MPS must be "activated" to facilitate generation of $SO_4^{\bullet-}$ from MPS. While several techniques have been proposed to activate MPS, usage of transition metals, such as cobalt (Co), has been validated as the most effective technique for activating MPS [15-17]. Therefore, a few studies have adopted homogeneous Co ions, or immobilized Co on substrates as catalysts for activating MPS [18-28]. Although Co ions or Co-immobilized materials could activate MPS, it is quite challenging to recover Co ions and also the immobilization of Co onto substrates is sophisticated [29, 30], rendering these catalysts less realistic to activate MPS for degrading emerging contaminants.

Even though cobalt oxides (e.g., Co_3O_4) have been also regarded as alternative heterogeneous catalysts for activating MPS, cobalt sulfides have also gained growing interests as cobalt sulfides possess interesting redox characteristics [31], making cobalt sulfides advantageous heterogeneous catalysts for activation MPS [32]. For example, a series of cobalt sulfides with different structures have been fabricated to activate MPS for eliminating antibiotics [32]. Unfortunately, studies of using cobalt sulfides for activating MPS are still very few, and no studies have been conducted to investigate cobalt sulfides for activating MPS to degrade 4HBP. Thus, the aim of this study is to develop and investigate cobalt sulfides for activating MPS to degrade 4HBP. Especially, a novel and interesting technique is adopted using Prussian Blue in the form of $Co_3[Co(CN)_6]_2$ as a precursor which could be sulfurized and converted into cobalt sulfides. With the cubic morphology of PB, the resultant cobalt sulfide originated from PB can still exhibit the cubic morphology but its faces have been transformed into nanofilms. Such a cubic assembly of cobalt sulfide nanofilms (CSNF) should be an interesting and promising heterogeneous catalyst for activating MPS to degrade 4HBP. Since no such catalyst has been even developed for activating MPS, the findings of this

study would provide useful insights into design, characterization and application of CSNF for degradation of chemical UV filters by $SO_4^{\bullet-}$-based AOPs.

2. Experimental

2.1 Preparation of Prussian Blue (PB) cubes of $Co_3[Co(CN)_6]_2$

Preparation of CSNF can be illustrated as shown in Fig. 1 from conversion of PB to CSNF via direct sulfurization of PB. In this study, all chemicals employed here were commercially available and used as received without additional purification. PB cubes were fabricated via a co-precipitation method based on the literature [33]. Firstly, 8.73 g $Co(NO_3)_2 \cdot 6H_2O$ and 13.24 g citric acid were dissolved in 1 L of DI water to obtain a solution A. Next, 6.65 g of $K_3[Co(CN)_6]$ was added in another 1 L of DI water to afford a solution B. The solution B was then gradually poured into the solution A under magnetic stirring for 10 min, and the resulting mixture was left without stirring at ambient temperature for 24 hr. The resulting precipitate was collected by centrifugation, washed with DI water/ethanol thoroughly, and dried in oven at 80 ℃ overnight to produce PB cubes of $Co_3[Co(CN)_6]_2$.

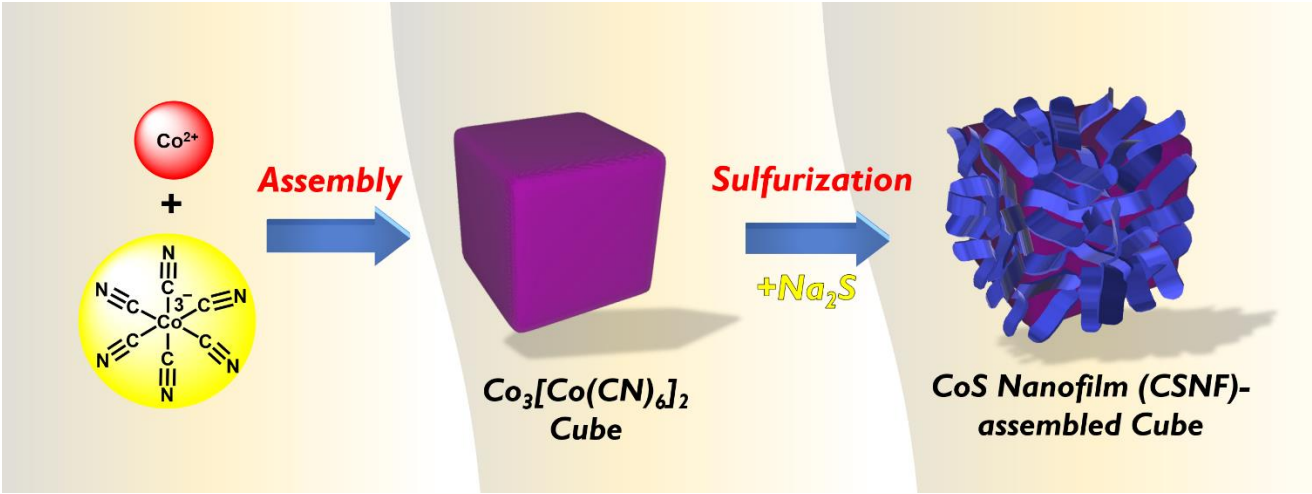

Fig. 1. Illustration of preparation of CSNF derived from sulfurization of Prussian Blue.

2.2 Preparation of CoS nanofilm (CSNF)

The as-prepared PB cubes (0.2 g) were re-dispersed in 200 mL of ethanol under vigorous stirring for 10 min to form a suspension. Subsequently, 2 g of Na_2S was dissolved in another 100 mL of DI water. Next, the Na_2S solution was dropwise added into the aforementioned PB suspension under stirring at 25 ℃ for 12 h, and then the sulfurized PB was collected by filtration, washed with DI water and ethanol, and dried in oven at 80 ℃ to produce CoS nanofilm (CSNF).

The morphology of catalysts were obtained by scanning and transmission electronic microscopies (JEOL, Japan), and its textural property was measured using a volumetric analyzer (Anton Paar Autosorb IQ, Austria). The XRD patterns of catalysts were then analyzed by an X-ray diffractometer (Bruker, USA), and its chemical composition was determined by energy-dispersive X-ray spectroscopy (EDS) (Oxford Instruments, UK), X-ray photoelectron spectroscopy (ULVAC-PHI, Japan), and Raman spectroscopy (TII, Japan). Surface charges of CSNF were measured by a zeta sizer (Malvern, UK).

2.3 Activation of MPS by CSNF for degradation of 4HBP.

4HBP degradation using MPS activated by CSNF was investigated by batch experiments. In a typical experiment, 20 mg of MPS was added into 200 mL of aqueous 4HBP solution with an initial concentration (C_0) of 5 mg/L. Subsequently, 10 mg of CSNF was added to the 4HBP solution at a constant temperature. After preset intervals, sample aliquots were withdrawn from the 4HBP solution and filtrated by filters to separate catalysts. The concentration of 4HBP in the filtrate (C_t) was then determined by a UV-Vis spectrophotometer at 298 nm (Fig. S1). Electron paramagnetic resonance (EPR) (Bruker, Germany) was adopted to analyze radical species from MPS using 5,5-Dimethyl-1-pyrroline N-oxide (DMPO) as a radical-trapping agent. The reusability of

CSNF for activation of MPS was verified by reusing CSNF for multi-cycle 4HBP degradation experiments. Commercial Co_3O_4 NP (*ca*. 50~80 nm) (Sigma-Aldrich, USA) was also acquired for comparing with CSNF. 4HBP degradation intermediates were determined by a mass spectrometer (Thermo Finnigan Corporation, LCQ ion-trap mass spectrometer, USA).

3. Results and Discussion

3.1 Characterization of CSNF

Since CSNF was derived from PB of $Co_3[Co(CN)_6]_2$, the morphology of PB was then visualized in Fig. 2(a-b), in which cubic structures can be observed. Its corresponding XRD pattern was also determined in Fig. 3, which could be correctly indexed to the pattern of PB [34, 35], confirming that PB was successfully formed with the cubic morphology.

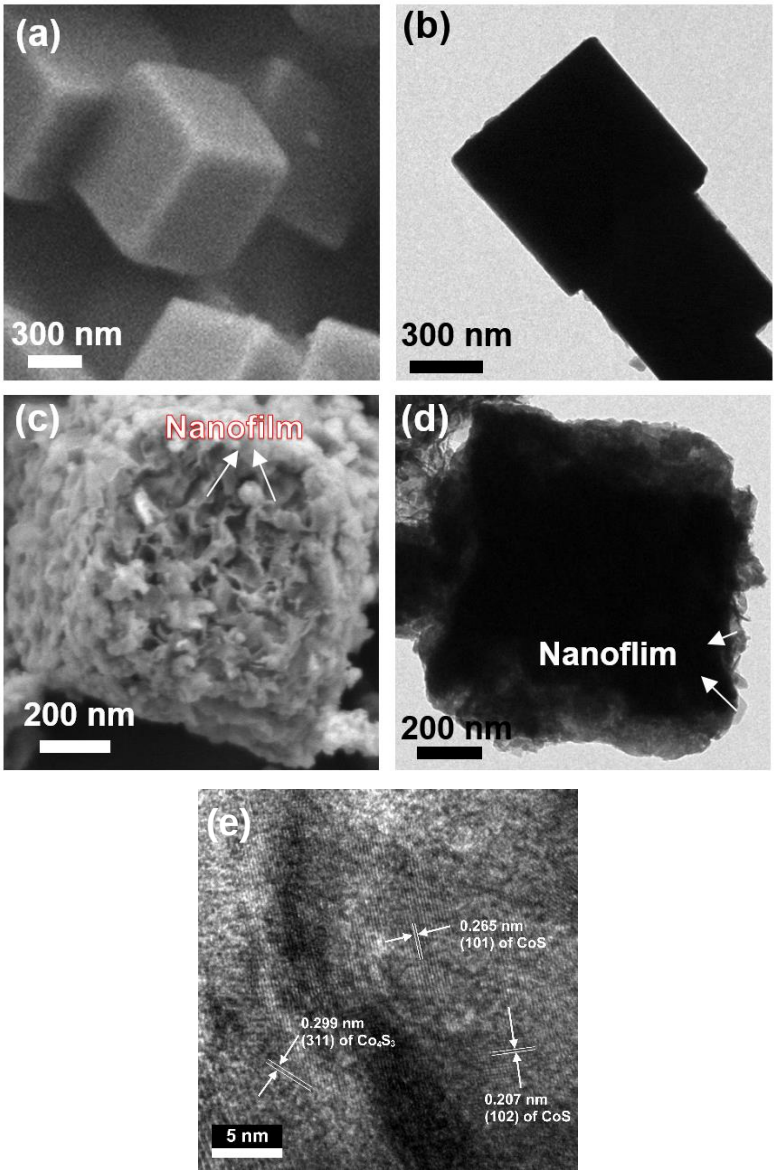

Fig. 2. (a) SEM and (b) TEM images of PB of $Co_3[Co(CN)_6]_2$; (c) SEM, (d) TEM , and (e) HRTEM images of CSNF.

Once PB was sulfurization, the resultant product was then shown in Fig. 2(c). While the pristine PB exhibited smooth surfaces, the surface of sulfurized product of PB became roughened and wrinkled with fluffy nanofilms. The formation of CoS films could be attributed to a possible mechanism in which Na_2S would be dissociated into Na^+ and S^{2-} and S^{2-} would then exchange with $Co(CN)_6^{3-}$ of PB, leading to a "etching" effect to erode the surface of PB [36]. Subsequently, as CoS typically exhibits the film-like (or sheet-like) morphology [37-39], the resulting nanofilms of CoS can be observed

on the cube's surface while many voids can be also observed because of the aforementioned etching effect.

While film-like CoS had been reported in a few literatures, for instance, Yu et al. proposed the fabrication of thin films of CoS; however these CoS thin films must be deposited on glass substrates to retain its morphology [40]. On the other hand, Mane et al. also proposed to grow CoS thin films by a relatively complicated liquid-phase chemical growth method; however a glass substrate was also required to support the CoS thin films [41]. These previous studies indicate that the conventional methods for fabricating CoS thin films would necessitate glass substrates. On the contrary, the CoS thin films obtained here could be produced through a relatively simple method by direct sulfidation of PB at ambient temperature without requirement of any glass substrates, revealing the advantage of the proposed method in the study.

The TEM image (Fig. 2(d)) demonstrates that these wrinkled nanofilms of sulfurized PB were very thin. In addition, the HRTEM of CSNF had been obtained and displayed in Fig. 2(e). The lattice-resolved image indicates *d*-spacing of 0.265 nm, and 0.207 nm, corresponding to the (101) and (102) planes of CoS as observed in the XRD pattern. In addition, a *d*-spacing of 0.299 nm can be also detected and attributed to the plane (311) of Co_4S_3 as observed in the XRD pattern of CSNF, confirming the existence of CoS and Co_4S_3 in CSNF.

To further analyze chemical composition of this sulfurized PB, the EDS analysis was employed and shown in Fig. 3(a). Since the pristine PB did not comprise sulfur, a notable signal of S could be observed in the sulfurized PB, verifying that PB had been modified with sulfur.

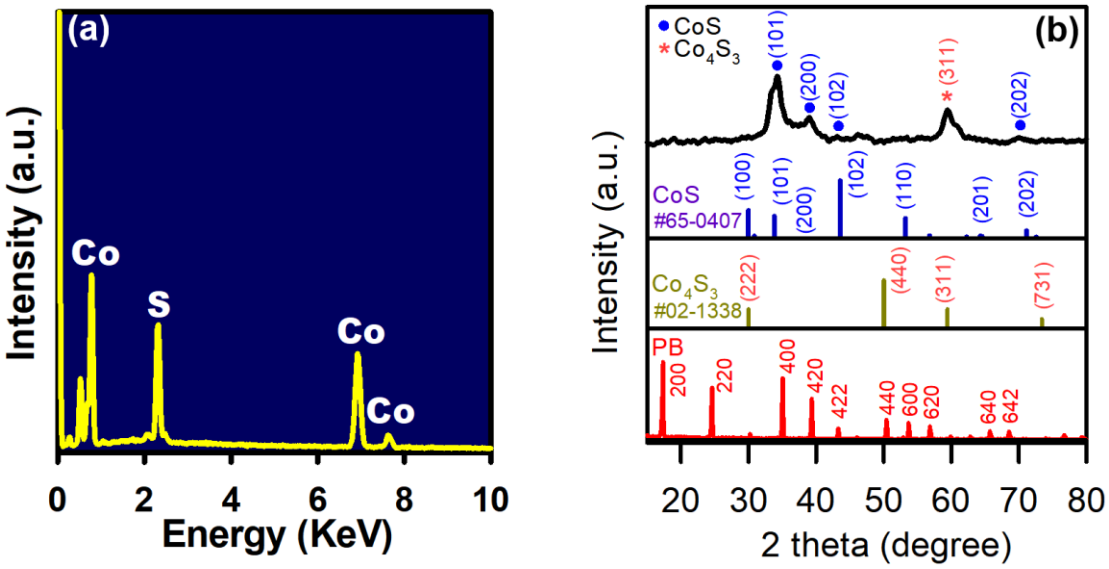

Fig. 3. (a) EDS analysis of CSNF; (b) XRD patterns of and CSNF and PB.

The corresponding XRD pattern of such a sulfurized PB can be seen in Fig. 3(b), and a number of significant peaks could be noticed at 34.3, 38.9, 46.4, and 59.6°. In particular, the peaks at 34.3, 38.9, and 46.4° would be ascribed to cobalt sulfide in the form of CoS (JCPDS #65-0407), whereas the peak at 59.6° corresponded to cobalt sulfide in the form of Co_4S_3 (JCPDS #02-1338), demonstrating that the sulfurized product of PB ($Co_3[Co(CN)_6]_2$) had been transformed into cobalt sulfides. As cobalt sulfides can exist in many forms, cobalt-sulfide-containing materials would usually contain partial patterns of various cobalt sulfides rather than exhibiting a full-set of XRD patterns of each species. For instance, Ahn et al. reported a composite of cobalt sulfide and rGO, and its corresponding XRD pattern comprised partial patterns of Co_3S_4, and CoS_2 and Co_3S_4 [42]. Similar results can be obtained in the study by Ma et al. for proposing a mixture of CoS and CoS_2 as an electrocatalyst [43]. In view of these standard peaks of cobalt sulfides, the XRD peaks of CSNF could be attributed to CoS and Co_4S_3.

These characteristics demonstrated that the PB cube had been transformed into cubic assembly of CoS nanofilms (CSNF) via the direct sulfurization of PB. Moreover,

Fig. 4 displays that Co and S elements were homogeneously distributed all over this cubic assembly of CSNFs, indicating that the entire pristine PB cube was thoroughly sulfurized, and transferred into cobalt sulfides.

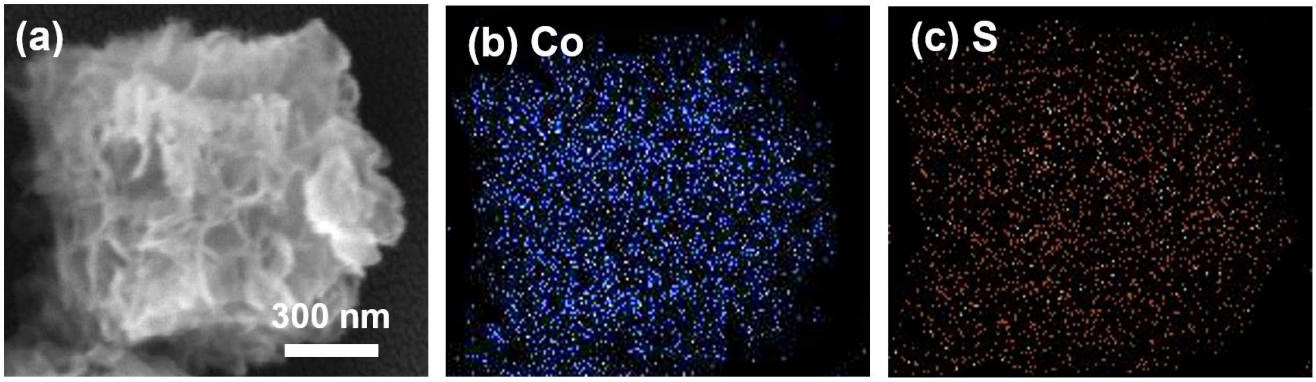

Fig. 4. Elemental mapping analyses of CSNF: (a) an image of selected region, (b) cobalt, and (c) sulfur.

Next, CSNF was analyzed by Raman spectroscopy in Fig. 5(a), and the corresponding Raman spectrum appeared to be quite different from that of the pristine PB. Four peaks were observed in the range from 150 to 700 cm^{-1}. Specifically, the peaks located at 194, and 523 can be attributed to the F_{2g} symmetry of Co [44, 45], whereas the peak at 485 cm^{-1} was derived from the E_g symmetry of Co. The high peak at 694 cm^{-1} corresponded to the A_{1g} symmetry of Co [46, 47].

Besides, the surface chemistry of CSNF was also investigated by XPS and its full spectrum (Fig. 5(b)) displays the significant signals of Co, and S. Moreover, the corresponding Co2p spectrum could be deconvoluted into several underlying peaks as Fig. 5(c). The peaks at 780.2 and 795.1 eV were attributed to Co^{3+}, while the peaks at 781.8 and 796.9 eV could be derived from Co^{2+} [48, 49]. The corresponding S2p XPS spectrum of CSNF was then revealed in Fig. 5(d), in which two peaks could be afforded after deconvolution. Specifically, the peak at 162.5 eV could be attributed to S^{2-} of

CSNF, and the peak in the range of 165~170 eV could be ascribed to S species in the inconsequential compounds of Co_xS_y in CSNF [50].

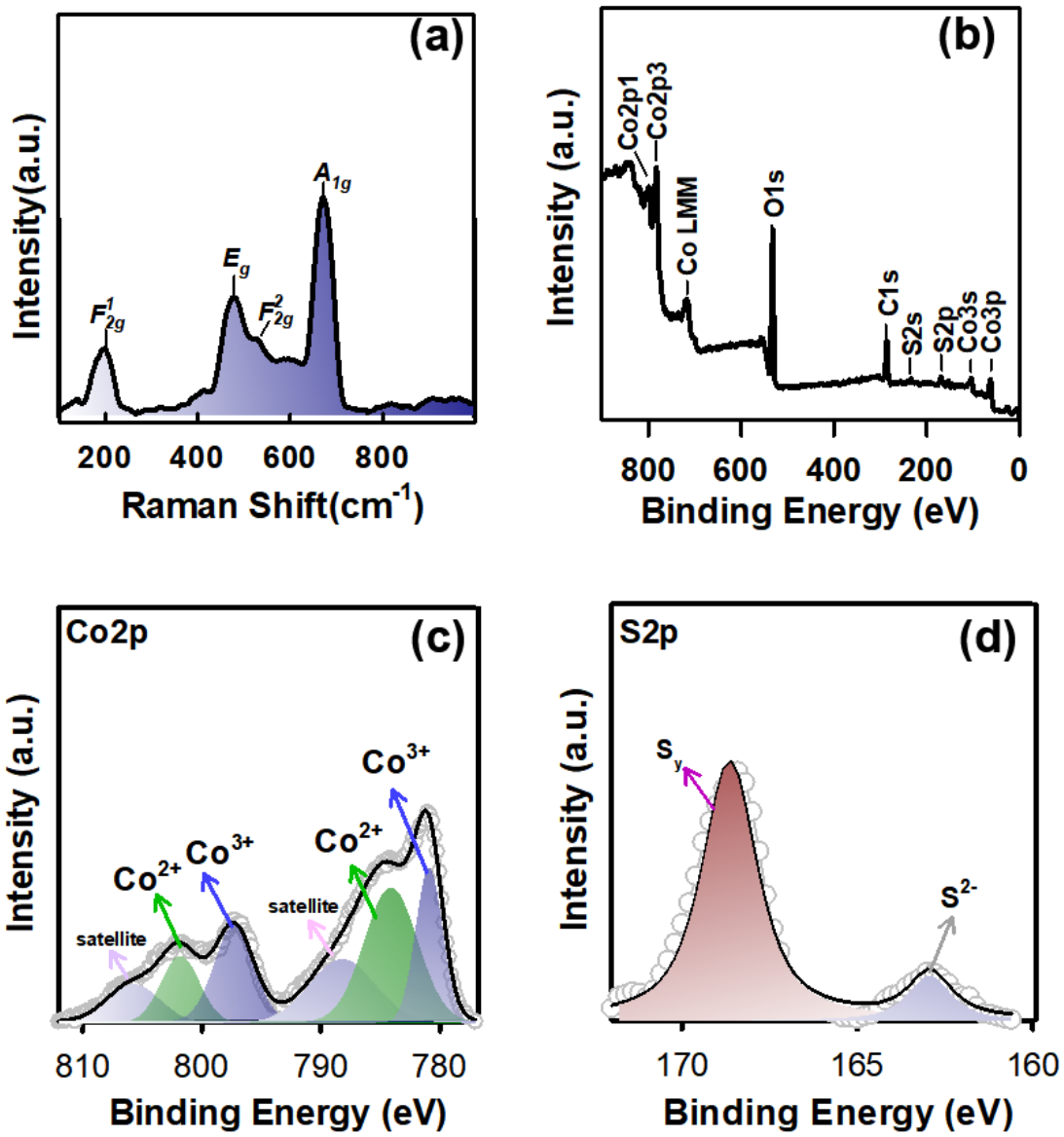

Fig. 5. (a) Raman spectra of CSNF and PB; (b) full survey, (c) Co2p, and (d) S2p XPS spectra of CSNF.

Since CSNF displayed a very unique morphology of cubic assembly of CSNF, its textural property was then measured by its N_2 sorption isotherms in Fig. 6(a). The isotherm seemed a combination of IUPAC type III and IV isotherms, suggesting that CSNF contained pores, potentially originated from inter-stacked nanofilms of CSNF as

observed in SEM images. Besides, a noticeable hysteresis loop was observed in the isotherm, validating the presence of mesopores in CSNF. Fig. 6(b) further verified that CSNF comprised mesopores and macropores, and the BET surface area of CSNF was 34 m^2/g with a pore volume of 0.16 cm^3/g.

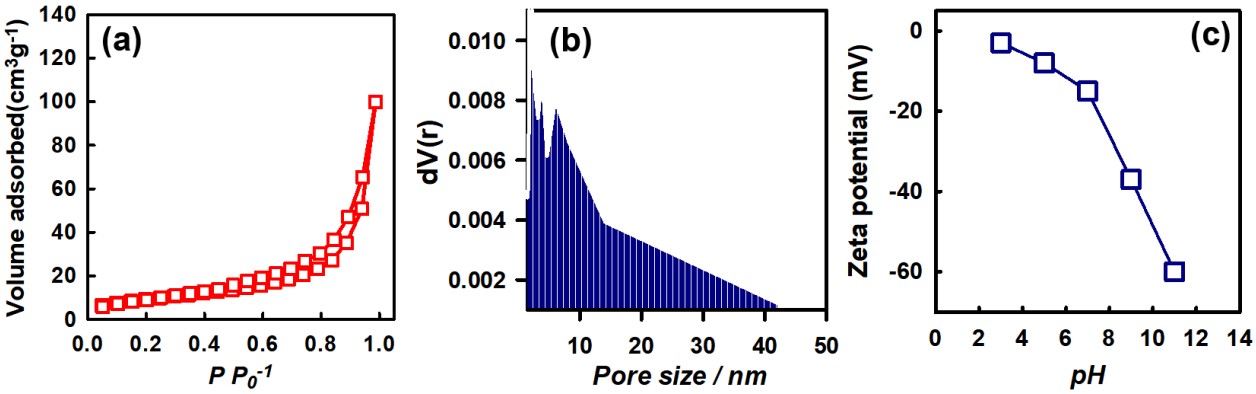

Fig. 6. Physical properties of CSNF: (a) N_2 sorption isotherm, (b) pore size distribution, and (c) zeta potential.

As MPS activation and 4HBP degradation were aqueous reactions, it was essential to realize the surface charges of CSNF in water as a function of pH. Fig. 6(c) shows that the surface charge of CSNF was -5 mV at pH = 3 and then reduced to -10 mV at pH = 5. At higher pH = 7, 9 and 11, zeta potentials further dropped to -17, -38, and -62 mV, respectively. This demonstrates that the surface charge of CSNF was negative under the neutral condition.

3.2 4HBP degradation by MPS activated using CSNF

Before evaluating 4HBP degradation using MPS activated by CSNF (CSNF+MPS), it was essential to examine if CSNF itself could eliminate 4HBP from water via adsorption. Fig. 7 displays that the concentration of 4HBP was almost unchanged in 45 min, indicating that CSNF was unable to eliminate 4HBP via adsorption. Moreover, it was also critical to verify whether MPS itself would degrade 4HBP; however, 4HBP

was negligibly eliminated in 45 min, demonstrating that MPS itself was unable to degrade 4HBP without proper activation of MPS.

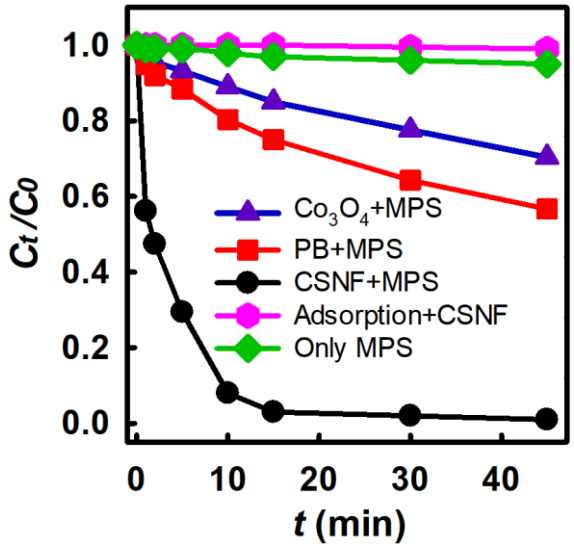

Fig. 7: Degradation of 4HBP by MPS, adsorption to CSNF, CSNF +MPS, PB+MPS and Co_3O_4 NP+MPS (Catalyst = 50 mg/L, MPS =100 mg/L ,T = 30 ℃).

When CSNF and MPS were both present in the 4HBP solution, the concentration of 4HBP rapidly decreased and C_t/C_0 approached zero within 45 min, demonstrating that CSNF+MPS completely eliminated 4HBP. Since CSNF and MPS were unable to degrade 4HBP separately, this full and rapid elimination of 4HBP by CSNF+MPS suggested that MPS was successfully activated by CSNF.

In consideration of Co^{2+} and Co^{3+} contained in CSNF, these Co species would react with MPS to produce sulfate radicals as follows (Eqs.(1)-(2)) [51, 52]:

$$Co^{2+}@CSNF + HSO_5^- \rightarrow Co^{3+}@CSNF + SO_4^{\bullet-} + OH^- \quad (1)$$

$$Co^{3+}@CSNF \rightarrow Co^{2+}@CSNF + SO_5^{\bullet-} + H^+ \quad (2)$$

As MPS was activated in the presence of CSNF for degrading 4HBP, it would be interesting to compare CSNF with its precursor, PB, for activating MPS. When PB and MPS were both present in the 4HBP solution, the concentration of 4HBP gradually decreased as C_t/C_0 at 45 min approached 0.58, indicating that the pristine PB could also

activate MPS for degrading 4HBP. However, the catalytic activity of PB was apparently much lower than its sulfurized derivative, CSNF, as 4HBP could not be eliminated and degradation kinetics was much slower using PB+MPS.

To quantify kinetics of 4HBP degradation, the pseudo first order model, which has intensively adopted to calculate rate constants of MPS-based degradation, was used as follows (Eq. (4)) [53]:

$$C_t = C_0 \exp(-kt) \quad (3)$$

where k represents the rate constant (min^{-1}). Since the rate constant (k) of 4HBP degradation by CSNF+MPS was 0.2335 min^{-1} (see Table S1 in the supporting information), the corresponding k by PB+MPS was 0.0125 min^{-1}, indicating that CSNF possessed a much higher catalytic activity, and the sulfurization could significantly improve catalytic activities of PB.

Moreover, while CSNF could successfully activate MPS, and surpassed PB for activating MPS to degrade 4HBP, it was important to compare it with the reference catalyst for MPS activation, Co_3O_4. Therefore, the commercial Co_3O_4 NP (Fig. S2) was purchased and compared with CSNF for MPS activation (Fig. 7). When Co_3O_4 NP seemed capable of activating MPS, 4HBP could not be fully eliminated in 45 min as the corresponding C_t/C_0 of 4HBP at 45 min merely reach 0.7. In addition, the reaction stoichiometric efficiency (RSE) was calculated at 45 min (Fig. S2). RSE averages ranged between 0.0148 and 0.0495; the highest RSE was for CSNF+MPS while the lowest RSE was Co_3O_4+MPS. From the results of RSE which can provide more clear comparisons proved CSNF can activate MPS more effectively again. This comparison validated that CSNF was also more efficient than Co_3O_4 NP, and CSNF was proven as an advantageous catalyst for activating MPS to degrade 4HBP.

Z. Yu et al. [54] and R. S. Mane et al. [55] have reported that different CoS films

prepared ways. Compared with previous reports, the CoS film in this research synthesis in room temperature which could avoid unnecessary energy waste and save process cost. Moreover, using the cubic morphology of PB as precursor to make CoS can still exhibit the cubic morphology though its faces have been transformed into nanofilms. Firstly, it could form more surface area for activating MPS to degrade 4HBP. On the other hand, it could also be observed from the degradation results that the use of PB to synthesize CoS can significantly improve its efficiency as a catalyst.

3.3 Effects of CSNF and MPS dosages on 4HBP degradation

While the combination of CSNF and MPS rapidly degraded 4HBP in 45 min, it was necessary to further distinguish their respective contributions. Therefore, effects of CSNF and MPS dosages on 4HBP degradation were studied. Fig. 8(a) displayed 4HBP degradation by CSNF at different dosages (25, 50, and 100 mg/L) with a fixed MPS dosage (100 mg/L). With these three CSNF dosages, CSNF could all quickly and fully eliminate 4HBP in 45 min; however, the degradation kinetics appeared very different with various CSNF dosages. In particular, as CSNF increased from 25 to 50 mg/L, k changed from 0.0948 to 0.2335 min^{-1}. When CSNF further increased to 100 mg/L, k was boosted to 1.2800 min^{-1}. These results validated that a higher dosage of CSNF significantly enhanced 4HBP degradation because more catalytic sites were available to accelerate MPS activation for faster 4HBP degradation.

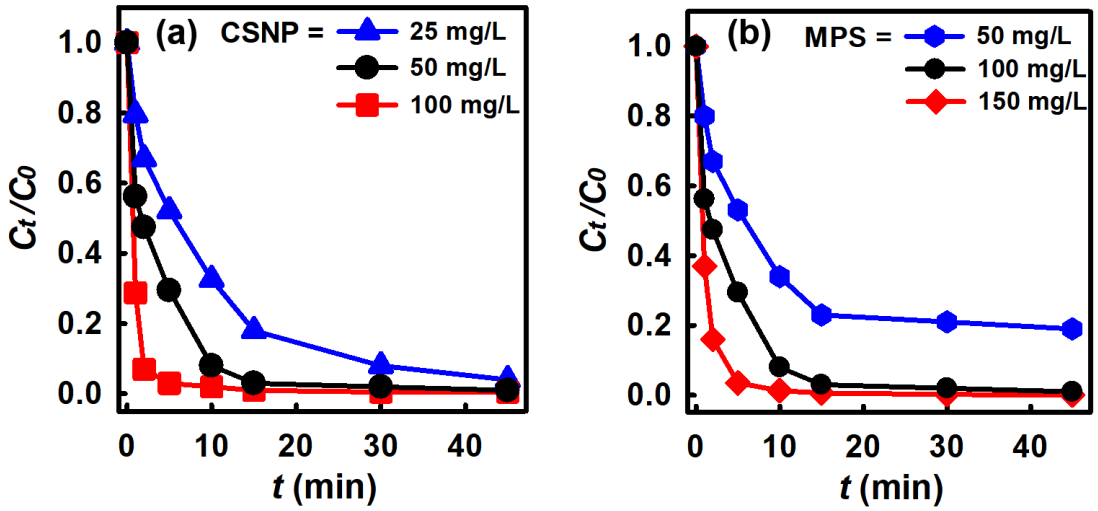

Fig. 8. Degradation of 4HBP by CSNF+MPS: (a) effect of CSNF dosage (MPS =100 mg/L ,T = 30 ℃), and (b) effect of MPS dosage (CSNF =50 mg/L ,T = 30 ℃).

Furthermore, 4HBP degradation by MPS at different dosages was also investigated in Fig. 8(b). As MPS dosage was increased from 100 to 150 mg/L, 4HBP degradation was also expedited as k increased from 0.2335 to 0.8892 min^{-1}. However, when MPS dosage was reduced from 100 to 50 mg/L, 4HBP degradation became much slower as k decreased from 0.2335 to 0.0604, and C_t/C_0 merely reached 0.2 in 45 min. These comparisons also suggested that the degradation extent of 4HBP was greatly correlated to MPS dosages as sulfate radicals are generated from MPS instead of catalysts. On the contrary, CSNF served as a catalyst which would manipulate degradation kinetics [56, 57].

3.4 Effects of temperature and initial pH on 4HBP degradation

Since temperature has been an important parameter for MPS activation, the effect of reaction temperature on 4HBP degradation by CSNF+MPS was then investigated. Fig. 9(a) displays 4HBP degradation by CSNF+MPS at 30, 40 and 50 °C. At these temperatures, 4HBP could be all eliminated fully; however, the degradation kinetics at

different temperatures were noticeably different. In particular, as temperature increased from 30 to 40 and 50 °C, k increased from 0.2335 to 0.5741 and 1.2600 min^{-1}, respectively, demonstrating that the higher temperatures could expedite 4HBP degradation by CSNF+MPS.

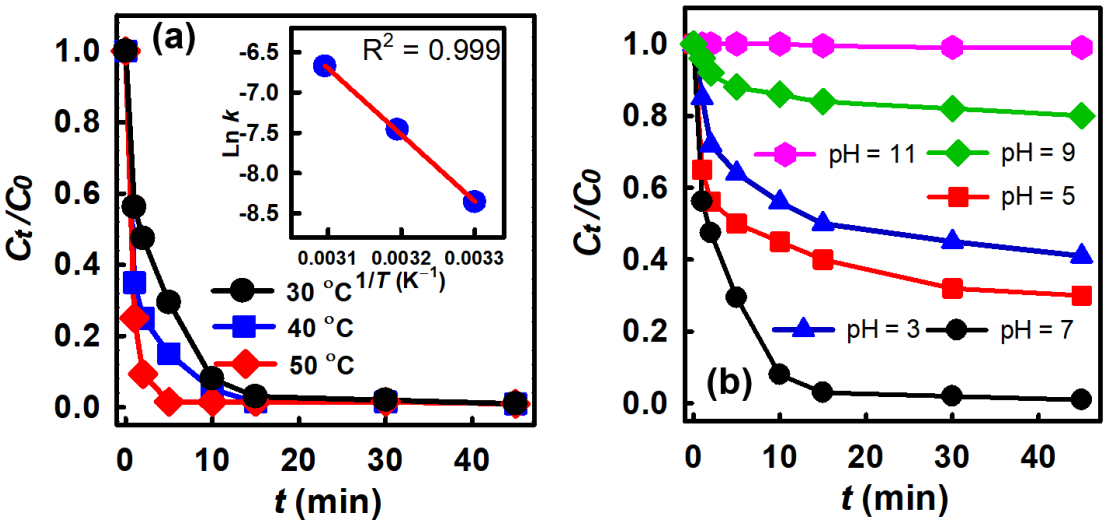

Fig. 9. Degradation of 4HBP by CSNF+MPS: (a) effect of temperature (CSNF =50 mg/L; MPS =100 mg/L), and (b) effect of pH value (CSNF = 50 mg/L; MPS =100 mg/L; T = 30 ℃).

In consideration of quicker kinetics at higher temperatures, k was then associated with temperature through the following Arrhenius equation (Eq.(5)):

$$\text{Ln } k = \ln A - E_a/RT \qquad (5)$$

where E_a is the activation energy (E_a, kJ/mol) of 4HBP degradation. A plot of $1/T$ vs. Ln k was revealed as the inset in Fig. 9(a) and the data points were properly fit by the linear regression with R^2 = 0.999 and then E_a was calculated as 68 kJ/mol.

Moreover, as MPS activation and 4HBP degradation were both aqueous reactions, pH value of 4HBP solution was a crucial factor and the effect of pH was then examined in Fig. 9(b). As the 4HBP solution was weakly acidic at pH = 5, 4HBP degradation by

CSNF+MPS was noticeably influenced as *k* decreased from 0.2335 to 0.0231 min^{-1}. When 4HBP solution became highly acidic at pH = 3, the adverse effect on 4HBP degradation became more pronounced as the corrsponding *k* decreased to 0.0188 min^{-1}, and only 60% of 4HBP was eliminated in 45 min. This demonstrated that acidic conditions would hinder MPS activation possibly due to the fact that MPS would become much more stable under acidic conditions [58], making MPS much more difficult to activate.

Besides, as the 4HBP solution became weakly basic at pH = 9, 4HBP degradation was significantly influenced as *k* decreased from 0.2335 to 0.0042 min^{-1}, and merely 20% of 4HBP was removed in 45 min. Once pH further increased to 11, 4HBP degradation was almost completely inhibited (with a significantly low *k* of 0.0003 min^{-1}). This could be possibly due to the reason that MPS would self-decompose without generation of $SO_4^{\bullet-}$ under basic conditions [58, 59], and insufficient $SO_4^{\bullet-}$ was generated to degrade 4HBP. Besides, the basic condition would make the surface of CSNF much more negative due to accumulation of OH^-. As a result, the electrostatic revulsion between 4HBP and the surface of CSNF became more intense, hindering $SO_5^{\bullet-}$ from reacting CSNF and restraining generation of $SO_4^{\bullet-}$.

3.5 The recyclability of CSNF for activating MPS to degrade 4HBP

Since CSNF was adopted as a heterogeneous catalyst for activating MPS to degrade 4HBP, it was essential to study whether CSNF could be reusable to activate MPS for 4HBP degradation. Fig. 10(a) further reveals that 4HBP was fully and quickly eliminated by reusing CSNF to activate MPS for consecutive 4 cycles. This verifies that

the used CSNF still exhibited stable and efficient catalytic activities for MPS activation to degrade 4HBP.

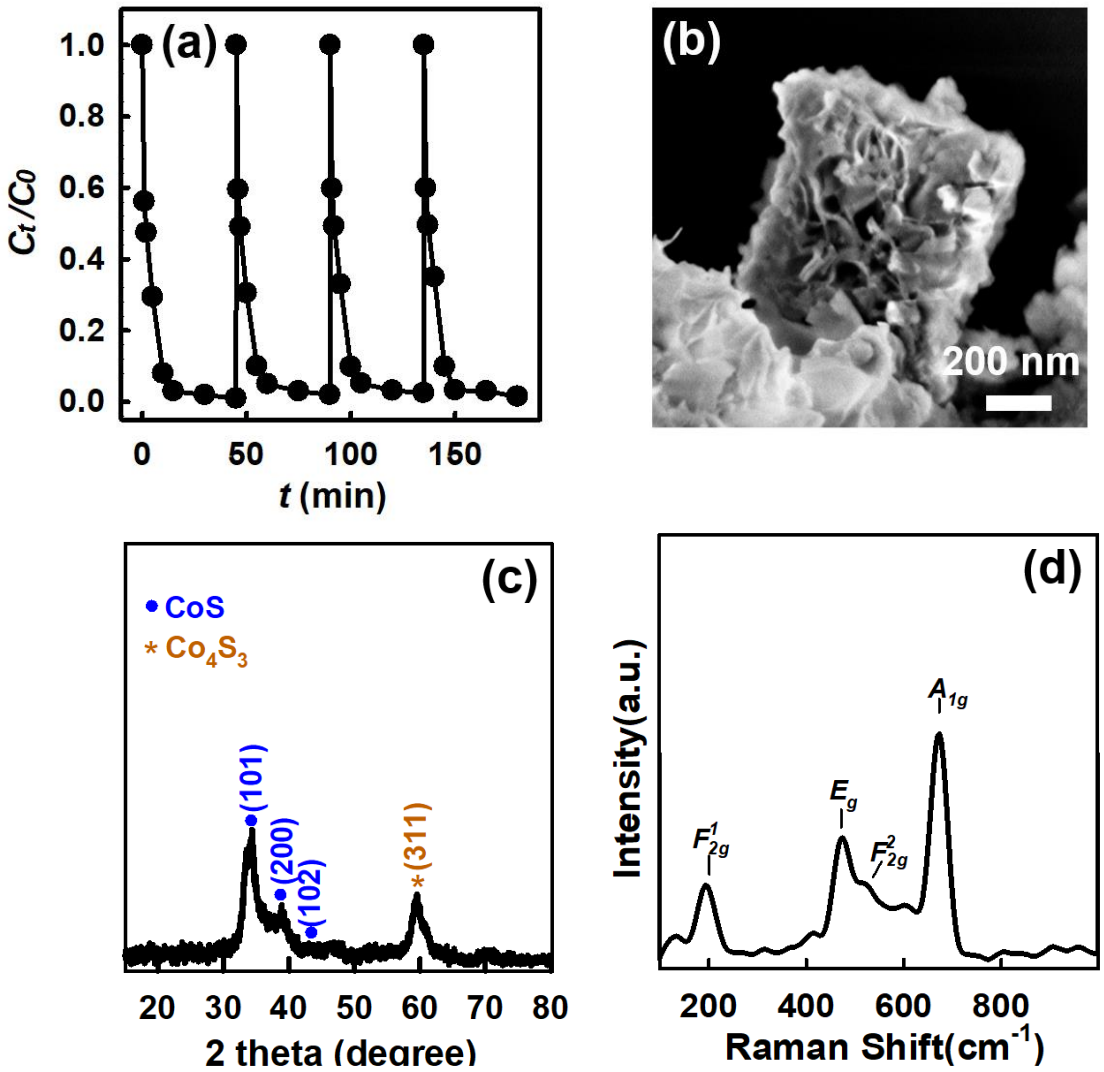

Fig. 10. (a) recyclability test of CSNF for degradation of DHB (CSNF =50 mg/L; MPS =100 mg/L; T = 30 ℃); (b) SEM image, (c) XRD pattern and (d) Raman spectrum of the spent CSNF.

The used CSNF was also analyzed and the SEM image of used CSNF still exhibited a cubic morphology with fluffy nanofilms on its surface, validating that the morphology of CSNF remained similar after the reaction. In addition, its XRD pattern (Fig. 10(b)) was very comparable to that of the pristine CSNF. In addition, the Raman spectrum of the used CSNF was also similar to that of the pristine CSNF. These features

validated that the characteristics of CSNF were remained without significant changes, and CSNF shall be a durable and reusable catalyst.

3.6 A proposed mechanism of 4HBP degradation by CSNF-activated MPS

Since MPS activation would generate $SO_4^{\bullet-}$, $SO_4^{\bullet-}$ could also react with water molecules to produce $^{\bullet}OH$ through the following [60] (Eq. (4)):

$$SO_4^{\bullet-} + H_2O \rightarrow SO_4^{2-} + {}^{\bullet}OH + H^+ \qquad (4)$$

Therefore, it was critical to examine whether these reactive oxygen species (*i.e.*, $^{\bullet}OH$ and $SO_4^{\bullet-}$) would be present and involved in 4HBP degradation by CSNF+MPS. To this end, two special radical scavengers were selected: *tert*-butanol and methanol. Since *tert*-butanol does not comprise *α*-hydrogen, it would react with $^{\bullet}OH$ quickly, making *tert*-butanol a radical probing reagent for $^{\bullet}OH$. Fig. 11(a) reveals that 4HBP degradation by CSNF+MPS in the presence of *tert*-butanol was greatly influenced and inhibited as *k* noticeably reduced from 0.2335 to 0.0109 min^{-1}, and merely 50% of 4HBP was eliminated in 45 min, indicating that $^{\bullet}OH$ seemed to involve in 4HBP degradation.

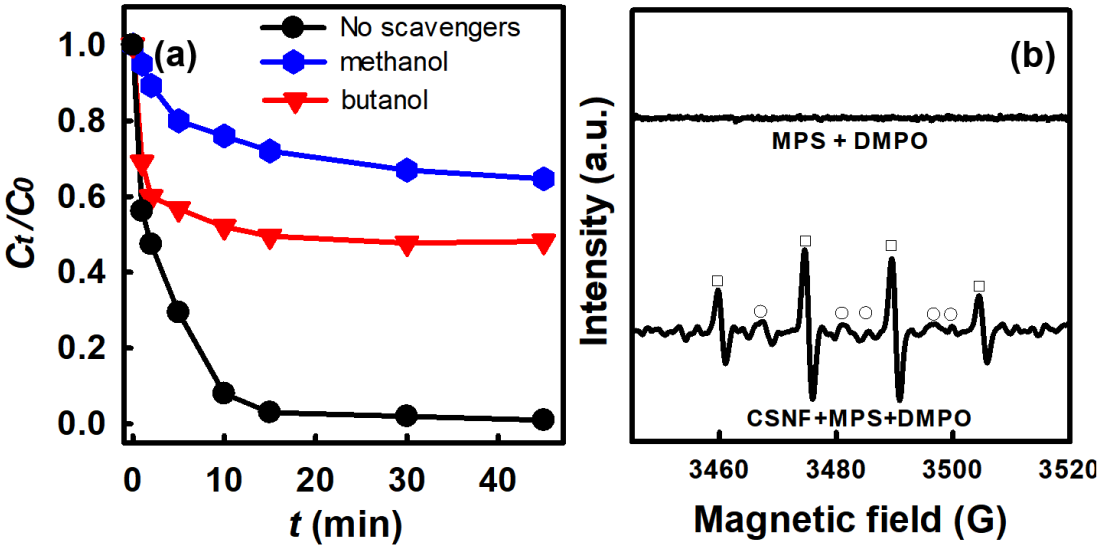

Fig. 11. (a) Effects of radical scavengers on 4HBP degradation (CSNF= 50 mg/L; MPS =100 mg/L; T = 30 ℃); (b) EPR analysis ((□: DMPO-$OH^{\bullet}$; ○: DMPO- $SO_4^{\bullet-}$).

Moreover, another radical probing reagent, methanol, was also examined as methanol consisting of α-hydrogen can rapidly react with both $OH^{\bullet}$ and $SO_4^{\bullet-}$ [61]. Fig. 11(a) reveals that 4HBP degradation was ineffective with $k = 0.0093\ min^{-1}$. This result suggests that both $OH^{\bullet}$ and $SO_4^{\bullet-}$ were present in CSNF+MPS, participating in 4HBP degradation.

For further verifying radical species generated from CSNF+MPS, EPR analysis was adopted as shown in Fig. 11(b). As DMPO was adopted as a spin-trapping agent, no noticeable pattern was obtained in the mixture of MPS and DMPO. However, once MPS and CSNF were both mixed with DMPO, a noticeable pattern was gained, and ascribed to the hyperfine splitting of oxidation adduct products of DMPO-OH and DMPO-SO_4 [62-67]. This validates that 4HBP degradation could be involved with both $SO_4^{\bullet-}$ and $^{\bullet}OH$, generated from CSNF+MPS.

3.7 A potential degradation pathway for 4HBP by CSNF-activated MPS

For further realizing 4HBP degradation by CSNF+MPS, intermediates of 4HBP degradation were then determined by mass spectrometry and summarized in Table S2. In view of these intermediates, a potential degradation pathway of 4HBP by CSNF+MPS could be schemed in Fig. 12.

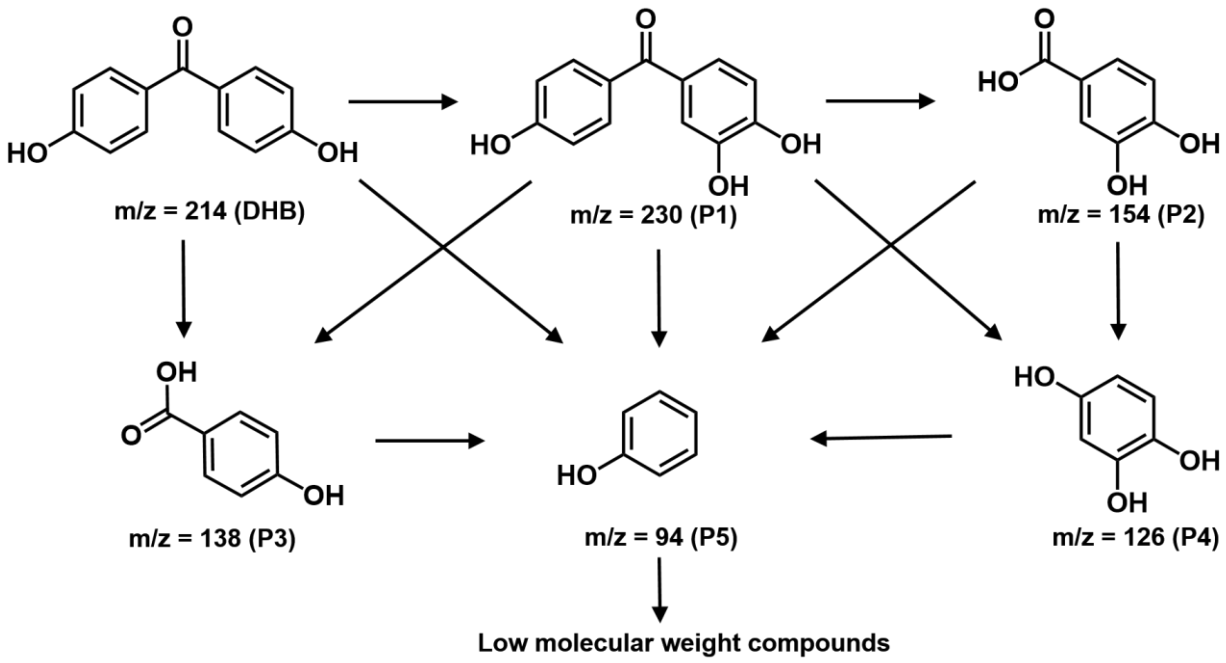

Fig. 12. A potential degradation pathway of 4HBP degradation by CSNF+MPS.

Initially, 4HBP might be oxidized by OH radicals to become P1 and its analogues. Next, P1 would be decomposed into P2 and P5, while P2 could be further oxidized into P4. Simultaneously, 4HBP would be also decomposed and broken into P3 and P5. Subsequently, P3 and P4 might be further decomposed to generate P5 or benzene rings, which were then oxidized and undergone ring-opening reactions to produce low-molecular-weight compounds eventually.

4. Conclusions

In this study, a unique cubic assembly of CoS nanofilm (CSNF) was fabricated via a convenient sulfurization of PB under the ambient condition to transform PB into cobalt sulfides. Such a resulting CSNF exhibited much higher catalytic activities than the pristine PB, and the reference catalyst, Co_3O_4, for activating MPS to degrade 4HBP. With very low dosages of CSNF = 50 mg/L and MPS = 100 mg/L, 5 mg/L of 4HBP could be fully eliminated in 15 min, validating that CSNF was a promising catalyst for activating MPS to 4HBP. E_a of 4HBP degradation by CSNF+MPS was also calculated

and the activation mechanism and degradation pathway of 4HBP degradation by CSNF+MPS was investigated here to provide insights into degradation behaviors for developing optimal sulfate-radical-based processes of 4HBP degradation.

References:

[1] D.L. Giokas, A. Salvador, A. Chisvert, UV filters: From sunscreens to human body and the environment, TrAC Trends in Analytical Chemistry, 26 (2007) 360-374.

[2] N.R. Janjua, B. Mogensen, A.-M. Andersson, J.H. Petersen, M. Henriksen, N.E. Skakkebæk, H.C. Wulf, Systemic Absorption of the Sunscreens Benzophenone-3, Octyl-Methoxycinnamate, and 3-(4-Methyl-Benzylidene) Camphor After Whole-Body Topical Application and Reproductive Hormone Levels in Humans, Journal of Investigative Dermatology, 123 (2004) 57-61.

[3] M.B. Ahmed, M.A.H. Johir, J.L. Zhou, H.H. Ngo, W. Guo, K. Sornalingam, Photolytic and photocatalytic degradation of organic UV filters in contaminated water, Current Opinion in Green and Sustainable Chemistry, 6 (2017) 85-92.

[4] H. Tinwell, P.A. Lefevre, G.J. Moffat, A. Burns, J. Odum, T.D. Spurway, G. Orphanides, J. Ashby, Confirmation of uterotrophic activity of 3-(4-methylbenzylidine)camphor in the immature rat, Environmental Health Perspectives, 110 (2002) 533-536.

[5] C. Schmutzler, I. Hamann, P.J. Hofmann, G. Kovacs, L. Stemmler, B. Mentrup, L. Schomburg, P. Ambrugger, A. Grüters, D. Seidlova-Wuttke, H. Jarry, W. Wuttke, J. Köhrle, Endocrine active compounds affect thyrotropin and thyroid hormone levels in serum as well as endpoints of thyroid hormone action in liver, heart and kidney, Toxicology, 205 (2004) 95-102.

[6] I. Tarazona, A. Chisvert, Z. León, A. Salvador, Determination of hydroxylated benzophenone UV filters in sea water samples by dispersive liquid–liquid microextraction followed by gas chromatography–mass spectrometry, Journal of Chromatography A, 1217 (2010) 4771-4778.

[7] M.E. Balmer, H.-R. Buser, M.D. Müller, T. Poiger, Occurrence of Some Organic UV Filters in Wastewater, in Surface Waters, and in Fish from Swiss Lakes, Environmental Science & Technology, 39 (2005) 953-962.

[8] M.M.P. Tsui, H.W. Leung, T.-C. Wai, N. Yamashita, S. Taniyasu, W. Liu, P.K.S. Lam, M.B. Murphy, Occurrence, distribution and ecological risk assessment of multiple classes of UV filters in surface waters from different countries, Water Research, 67 (2014) 55-65.

[9] X. Li, G. Chen, J. Liu, Y. Liu, X. Zhao, Z. Cao, L. Xia, G. Li, Z. Sun, S. Zhang, H. Wang, J. You, A rapid, accurate and sensitive method with the new stable isotopic tags based on microwave-assisted dispersive liquid-liquid microextraction and its application to the determination of hydroxyl UV filters in environmental water samples, Talanta, 167 (2017) 242-252.

[10] X. Zheng, X.-M. Ren, L. Zhao, L.-H. Guo, Binding and activation of estrogen related receptor γ as possible molecular initiating events of hydroxylated benzophenones endocrine disruption toxicity, Environmental Pollution, 263 (2020) 114656.

[11] J.A. Khan, M. Sayed, S. Khan, N.S. Shah, D.D. Dionysiou, G. Boczkaj, Chapter 9 - Advanced oxidation processes for the treatment of contaminants of emerging concern, in: A.J. Hernández-Maldonado, L. Blaney (Eds.) Contaminants of Emerging Concern in Water and Wastewater, Butterworth-Heinemann, 2020, pp. 299-365.

[12] S.A. Fast, V.G. Gude, D.D. Truax, J. Martin, B.S. Magbanua, A Critical Evaluation of Advanced Oxidation Processes for Emerging Contaminants Removal, Environmental Processes, 4 (2017) 283-302.

[13] T. Olmez-Hanci, I. Arslan-Alaton, Comparison of sulfate and hydroxyl radical based advanced oxidation of phenol, Chemical Engineering Journal, 224 (2013) 10-16.

[14] P. Hu, M. Long, Cobalt-catalyzed sulfate radical-based advanced oxidation: A review on heterogeneous catalysts and applications, Applied Catalysis B: Environmental, 181 (2016) 103-117.

[15] G.P. Anipsitakis, E. Stathatos, D.D. Dionysiou, Heterogeneous Activation of Oxone Using Co3O4, The Journal of Physical Chemistry B, 109 (2005) 13052-13055.

[16] G. Wei, X. Liang, Z. He, Y. Liao, Z. Xie, P. Liu, S. Ji, H. He, D. Li, J. Zhang, Heterogeneous activation of Oxone by substituted magnetites Fe3−xMxO4 (Cr, Mn, Co, Ni) for degradation of Acid Orange II at neutral pH, Journal of Molecular Catalysis A: Chemical, 398 (2015) 86-94.

[17] Z. Li, Z. Chen, Y. Xiang, L. Ling, J. Fang, C. Shang, D.D. Dionysiou, Bromate formation in bromide-containing water through the cobalt-mediated activation of peroxymonosulfate, Water Research, 83 (2015) 132-140.

[18] Q. Yang, H. Choi, S.R. Al-Abed, D.D. Dionysiou, Iron–cobalt mixed oxide nanocatalysts: Heterogeneous peroxymonosulfate activation, cobalt leaching, and ferromagnetic properties for environmental applications, Applied Catalysis B: Environmental, 88 (2009) 462-469.

[19] C. Cai, H. Zhang, X. Zhong, L. Hou, Ultrasound enhanced heterogeneous activation of peroxymonosulfate by a bimetallic Fe–Co/SBA-15 catalyst for the

degradation of Orange II in water, Journal of Hazardous Materials, 283 (2015) 70-79.

[20] H.-K. Lai, Y.-Z. Chou, M.-H. Lee, K.-Y.A. Lin, Coordination polymer-derived cobalt nanoparticle-embedded carbon nanocomposite as a magnetic multi-functional catalyst for energy generation and biomass conversion, Chemical Engineering Journal, 332 (2018) 717-726.

[21] M.-C. Li, S. Tong, J.-T. Lin, K.-Y.A. Lin, Y.-F. Lin, Electrospun Co3O4 nanofiber as an efficient heterogeneous catalyst for activating peroxymonosulfate in water, J Taiwan Inst Chem Eng, 106 (2020) 110-117.

[22] K.-Y.A. Lin, F.-K. Hsu, W.-D. Lee, Magnetic cobalt-graphene nanocomposite derived from self-assembly of MOFs with graphene oxide as an activator for peroxymonosulfate, Journal of Materials Chemistry A, 3 (2015) 9480-9490.

[23] K.-Y.A. Lin, S.-Y. Chen, Catalytic Reduction of Bromate Using ZIF-Derived Nanoscale Cobalt/Carbon Cages in the Presence of Sodium Borohydride, ACS Sustainable Chemistry & Engineering, 3 (2015) 3096-3103.

[24] K.-Y.A. Lin, J.-T. Lin, X.-Y. Lu, C. Hung, Y.-F. Lin, Electrospun magnetic cobalt-embedded carbon nanofiber as a heterogeneous catalyst for activation of oxone for degradation of Amaranth dye, Journal of Colloid and Interface Science, 505 (2017) 728-735.

[25] K.-Y.A. Lin, T.-Y. Lin, Degradation of Acid Azo Dyes Using Oxone Activated by Cobalt Titanate Perovskite, Water, Air, & Soil Pollution, 229:10 (2018).

[26] K.-Y.A. Lin, M.-T. Yang, J.-T. Lin, Y. Du, Cobalt ferrite nanoparticles supported on electrospun carbon fiber as a magnetic heterogeneous catalyst for activating peroxymonosulfate, Chemosphere, 208 (2018) 502-511.

[27] D.D. Tuan, W.D. Oh, F. Ghanbari, G. Lisak, S. Tong, K.-Y. Andrew Lin, Coordination polymer-derived cobalt-embedded and N/S-doped carbon nanosheet with a hexagonal core-shell nanostructure as an efficient catalyst for activation of oxone in water, J Colloid Interface Sci, 579 (2020) 109-118.

[28] W.-C. Yun, K.-Y.A. Lin, W.-C. Tong, Y.-F. Lin, Y. Du, Enhanced degradation of paracetamol in water using sulfate radical-based advanced oxidation processes catalyzed by 3-dimensional Co3O4 nanoflower, Chemical Engineering Journal, 373 (2019) 1329-1337.

[29] F. Qi, W. Chu, B. Xu, Catalytic degradation of caffeine in aqueous solutions by cobalt-MCM41 activation of peroxymonosulfate, Appl Catal B, 134–135 (2013) 324-332.

[30] F. Qi, W. Chu, B. Xu, Modeling the heterogeneous peroxymonosulfate/Co-MCM41 process for the degradation of caffeine and the study of influence of cobalt sources, Chemical Engineering Journal, 235 (2014) 10-18.

[31] Y. Sun, C. Liu, D.C. Grauer, J. Yano, J.R. Long, P. Yang, C.J. Chang, Electrodeposited Cobalt-Sulfide Catalyst for Electrochemical and Photoelectrochemical Hydrogen Generation from Water, J Am Chem Soc, 135 (2013) 17699-17702.

[32] W. Li, S. Li, Y. Tang, X. Yang, W. Zhang, X. Zhang, H. Chai, Y. Huang, Highly efficient activation of peroxymonosulfate by cobalt sulfide hollow nanospheres for fast ciprofloxacin degradation, Journal of Hazardous Materials, 389 (2020) 121856.

[33] S.-C. Wang, D. Xiong, C. Chen, M. Gu, F.-Y. Yi, The controlled fabrication of hierarchical CoS2@NiS2 core-shell nanocubes by utilizing prussian blue analogue for enhanced capacitive energy storage performance, Journal of Power Sources, 450 (2020).

[34] C.-H. Wu, Y.-T. Chiu, K.-Y.A. Lin, Macrosphere-supported nanoscale Prussian blue analogues prepared via self-assembly as multi-functional heterogeneous catalysts for aqueous oxidative and reductive reactions, Separation and Purification Technology, 199 (2018) 222-232.

[35] K.-Y.A. Lin, B.-J. Chen, C.-K. Chen, Evaluating Prussian blue analogues MII3[MIII(CN)6]2 (MII = Co, Cu, Fe, Mn, Ni; MIII = Co, Fe) as activators for peroxymonosulfate in water, RSC Adv, 6 (2016) 92923-92933.

[36] J. Liu, S. Wei, N. Li, L. Zhang, X. Cui, Delicate excavated trimetallic Prussian blue analogues for efficient oxygen evolution reactions, Electrochimica Acta, 299 (2019) 575-581.

[37] J. Lin, Y. Liu, Y. Wang, H. Jia, S. Chen, J. Qi, C. Qu, J. Cao, W. Fei, J. Feng, Rational construction of nickel cobalt sulfide nanoflakes on CoO nanosheets with the help of carbon layer as the battery-like electrode for supercapacitors, Journal of Power Sources, 362 (2017) 64-72.

[38] W. Fu, C. Zhao, W. Han, Y. Liu, H. Zhao, Y. Ma, E. Xie, Cobalt sulfide nanosheets coated on NiCo2S4 nanotube arrays as electrode materials for high-performance supercapacitors, Journal of Materials Chemistry A, 3 (2015) 10492-10497.

[39] S. Aloqayli, C.K. Ranaweera, Z. Wang, K. Siam, P.K. Kahol, P. Tripathi, O.N. Srivastava, B.K. Gupta, S.R. Mishra, F. Perez, X. Shen, R.K. Gupta, Nanostructured cobalt oxide and cobalt sulfide for flexible, high performance and durable supercapacitors, Energy Storage Materials, 8 (2017) 68-76.

[40] Z. Yu, J. Du, S. Guo, J. Zhang, Y. Matsumoto, CoS thin films prepared with modified chemical bath deposition, Thin Solid Films, 415 (2002) 173-176.

[41] S.T. Mane, S.S. Kamble, L.P. Deshmukh, Cobalt sulphide thin films: Chemical bath deposition, growth and properties, Materials Letters, 65 (2011) 2639-2641.

[42] S. Ahn, J. Yang, H. Lim, H.S. Shin, Selective synthesis of pure cobalt disulfide on reduced graphene oxide sheets and its high electrocatalytic activity for hydrogen evolution reaction, Nano Convergence, 3 (2016) 5.

[43] D. Ma, B. Hu, W. Wu, X. Liu, J. Zai, C. Shu, T. Tadesse Tsega, L. Chen, X. Qian, T.L. Liu, Highly active nanostructured CoS2/CoS heterojunction electrocatalysts for aqueous polysulfide/iodide redox flow batteries, Nature Communications, 10 (2019) 3367.

[44] S. Zhao, F. Hu, J. Li, Hierarchical Core–Shell Al2O3@Pd-CoAlO Microspheres for Low-Temperature Toluene Combustion, ACS Catalysis, 6 (2016) 3433-3441.

[45] B. de Rivas, R. López-Fonseca, C. Jiménez-González, J.I. Gutiérrez-Ortiz, Synthesis, characterisation and catalytic performance of nanocrystalline Co3O4 for gas-phase chlorinated VOC abatement, Journal of Catalysis, 281 (2011) 88-97.

[46] Q. Liu, L.-C. Wang, M. Chen, Y. Cao, H.-Y. He, K.-N. Fan, Dry citrate-precursor synthesized nanocrystalline cobalt oxide as highly active catalyst for total oxidation of propane, Journal of Catalysis, 263 (2009) 104-113.

[47] X. Wang, Y. Liu, T. Zhang, Y. Luo, Z. Lan, K. Zhang, J. Zuo, L. Jiang, R. Wang, Geometrical-Site-Dependent Catalytic Activity of Ordered Mesoporous Co-Based Spinel for Benzene Oxidation: In Situ DRIFTS Study Coupled with Raman and XAFS Spectroscopy, ACS Catalysis, 7 (2017) 1626-1636.

[48] L.-L. Feng, M. Fan, Y. Wu, Y. Liu, G.-D. Li, H. Chen, W. Chen, D. Wang, X. Zou, Metallic Co9S8 nanosheets grown on carbon cloth as efficient binder-free electrocatalysts for the hydrogen evolution reaction in neutral media, Journal of Materials Chemistry A, 4 (2016) 6860-6867.

[49] C. Dong, L. Guo, H. Li, B. Zhang, X. Gao, F. Tian, Y. Qian, D. Wang, L. Xu, Rational fabrication of CoS2/Co4S3@N-doped carbon microspheres as excellent cycling performance anode for half/full sodium ion batteries, Energy Storage Materials, 25 (2020) 679-686.

[50] S. Das, P. Sudhagar, S. Nagarajan, E. Ito, S.Y. Lee, Y.S. Kang, W. Choi, Synthesis of graphene-CoS electro-catalytic electrodes for dye sensitized solar cells, Carbon, 50 (2012) 4815-4821.

[51] S. Muhammad, E. Saputra, H. Sun, J.d.C. Izidoro, D.A. Fungaro, H.M. Ang, M.O. Tade, S. Wang, Coal fly ash supported Co3O4 catalysts for phenol degradation using peroxymonosulfate, RSC Advances, 2 (2012) 5645-5650.

[52] Y. Yao, Z. Yang, H. Sun, S. Wang, Hydrothermal Synthesis of Co3O4–Graphene for Heterogeneous Activation of Peroxymonosulfate for Decomposition of Phenol, Industrial & Engineering Chemistry Research, 51 (2012) 14958-14965.

[53] Q. Wang, Y. Shao, N. Gao, W. Chu, J. Chen, X. Lu, Y. Zhu, N. An, Activation of peroxymonosulfate by Al2O3-based CoFe2O4 for the degradation of sulfachloropyridazine sodium: Kinetics and mechanism, Separation and Purification Technology, 189 (2017) 176-185.

[54] Y.C. Tsai, N.N. Huy, D.C.W. Tsang, K.Y.A. Lin, Metal organic framework-derived 3D nanostructured cobalt oxide as an effective catalyst for soot oxidation.

[55] I.K.M. Yu, A. Hanif, D.C.W. Tsang, A.C.K. Yip, K.Y.A. Lin, B. Gao, Y.S. Ok, C.S. Poon, J. Shang, Tailoring acidity and porosity of alumina catalysts via transition metal doping for glucose conversion in biorefinery.

[56] C.-B. Chen, F. Zhang, C.-X. Li, J.-Y. Lu, S. Cui, H.-Q. Liu, W.-W. Li, A magnetic CoFe2O4-CNS nanocomposite as an efficient, recyclable catalyst for peroxymonosulfate activation and pollutant degradation, RSC Advances, 7 (2017) 55020-55025.

[57] Y. Pi, L. Ma, P. Zhao, Y. Cao, H. Gao, C. Wang, Q. Li, S. Dong, J. Sun, Facile green synthetic graphene-based Co-Fe Prussian blue analogues as an activator of peroxymonosulfate for the degradation of levofloxacin hydrochloride, Journal of Colloid and Interface Science, 526 (2018) 18-27.

[58] W. Guo, S. Su, C. Yi, Z. Ma, Degradation of antibiotics amoxicillin by Co3O4-catalyzed peroxymonosulfate system, Environmental Progress & Sustainable Energy, 32 (2013) 193-197.

[59] A. Rastogi, S.R. Al-Abed, D.D. Dionysiou, Sulfate radical-based ferrous–peroxymonosulfate oxidative system for PCBs degradation in aqueous and sediment systems, Applied Catalysis B: Environmental, 85 (2009) 171-179.

[60] L.J. Xu, W. Chu, L. Gan, Environmental application of graphene-based CoFe2O4 as an activator of peroxymonosulfate for the degradation of a plasticizer, Chemical Engineering Journal, 263 (2015) 435-443.

[61] Z. Huang, H. Bao, Y. Yao, W. Lu, W. Chen, Novel green activation processes and mechanism of peroxymonosulfate based on supported cobalt phthalocyanine catalyst, Applied Catalysis B: Environmental, 154–155 (2014) 36-43.

[62] S. Indrawirawan, H. Sun, X. Duan, S. Wang, Nanocarbons in different structural dimensions (0–3D) for phenol adsorption and metal-free catalytic oxidation, Applied Catalysis B: Environmental, 179 (2015) 352-362.

[63] A. Khan, S. Zou, T. Wang, J. Ifthikar, A. Jawad, Z. Liao, A. Shahzad, A. Ngambia, Z. Chen, Facile synthesis of yolk shell Mn2O3@Mn5O8 as an effective catalyst for peroxymonosulfate activation, Physical Chemistry Chemical Physics, 20 (2018) 13909-13919.

[64] L. Peng, X. Gong, X. Wang, Z. Yang, Y. Liu, In situ growth of ZIF-67 on a nickel foam as a three-dimensional heterogeneous catalyst for peroxymonosulfate activation, RSC Advances, 8 (2018) 26377-26382.

[65] R. Lan, W. Su, J. Li, Preparation and Catalytic Performance of Expanded Graphite for Oxidation of Organic Pollutant, Catalysts, 9 (2019) 280.

[66] A. Jawad, J. Lang, Z. Liao, A. Khan, J. Ifthikar, Z. Lv, S. Long, Z. Chen, Z. Chen, Activation of persulfate by CuOx@Co-LDH: A novel heterogeneous system for contaminant degradation with broad pH window and controlled leaching, Chemical Engineering Journal, 335 (2018) 548-559.

[67] X. Duan, K. O'Donnell, H. Sun, Y. Wang, S. Wang, Sulfur and Nitrogen Co-Doped Graphene for Metal-Free Catalytic Oxidation Reactions, Small, 11 (2015) 3036-3044.

Credit Author Statement

Jhih-Yang Yin: Data curation, Writing- Original draft preparation*; Wen Da Oh:* Writing-Original draft preparation; *Eilhann Kwon*: Data curation, Visualization, Investigation; *Siming You:* Writing- Reviewing and Editing; *Bui Xuan Thanh :* Visualization, Investigation; *Haitao Wang*: Visualization, Investigation; *Kun-Yi Andrew Lin :* Data curation, Writing- Original draft preparation